JOURNAL OF SOLID STATE CHEMISTRY 100, 101–114 (1992)

The Defect Structure of Anion-Excess $(Ca_{1-x}Y_x)F_{2+x}$ with $x = 0.06$

S. HULL* AND C. C. WILSON

The ISIS Facility, Rutherford Appleton Laboratory, Chilton, Didcot, Oxfordshire, OX11 0QX, United Kingdom

Received October 21, 1991; in revised form February 25, 1992; accepted March 3, 1992

The defect structure of the anion-excess fluorite $(Ca_{1-x}Y_x)F_{2+x}$ with $x = 0.06$ has been investigated using single-crystal neutron diffraction. Least-squares refinement of the measured Bragg intensities has been performed considering four positions for the disordered anions within the $Fm\bar{3}m$ unit cell: in 48*i* sites at $(\frac{1}{2}, u, u)$ with $u = 0.39$; in 32*f* sites at (w, w, w) with $w = 0.38$; in 32*f* sites at (v, v, v) with $v = 0.27$, and in the empty cube center 4*b* sites at $(\frac{1}{2}, \frac{1}{2}, \frac{1}{2})$. The results indicate that only the $(\frac{1}{2}, u, u)$ and (v, v, v) sites are significantly occupied. Information concerning the local defect configuration has been provided by least-squares refinement of the measured distribution of coherent elastic diffuse scattering within the $(1\bar{1}0)$ plane of reciprocal space. The best agreement with both Bragg diffraction and diffuse scattering data is obtained by adopting a model of randomly distributed cuboctahedral anion polyhedra, of the type observed in ordered anion-excess fluorite superlattices. © 1992 Academic Press, Inc.

1. Introduction

Halide compounds with the fluorite crystal structure, with general formula $M^{2+}X_2^-$, have a remarkable ability to accommodate large concentrations of trivalent R^{3+} dopant ions substitutionally on the M^{2+} cation sites. Overall charge neutrality in the doped system is maintained by incorporating excess X^- into the anion sublattice. The addition of R^{3+} ions dramatically reduces the transition temperature, T_c, above which high ionic conductivity is observed (*1*), and technological interest in solid electrolytes has led to considerable research effort aimed at understanding this effect and elucidating the structural changes which accompany doping. However, the detailed topology of the defect clusters formed in anion-excess fluorites is still the subject of some controversy, even in the most widely studied system, $(Ca_{1-x}Y_x)F_{2+x}$.

The fluorite structure (space group $Fm\bar{3}m$) is illustrated in Fig. 1, with the cations in 4*a* sites at (0, 0, 0) and anions in 8*c* sites at $(\frac{1}{4}, \frac{1}{4}, \frac{1}{4})$. The structure can most conveniently be considered as a simple cubic array of anions with cations occupying alternate cube centers. At relatively low R^{3+} dopant levels ($x < \sim 0.001$) charge compensation occurs by the formation of simple dopant-excess anion pairs, with interstitial anions situated in one of the empty cube centers at $(\frac{1}{2}, \frac{1}{2}, \frac{1}{2})$, either in nearest neighbor (*2*) or next nearest neighbor (*3*) positions. At higher dopant levels ($x \sim 0.01$–0.15) excess anions are accommodated in the form of discrete defect clusters, models for which are discussed in the following section. In this work the results of a single-crystal neutron diffraction study of the anion-excess fluorite compound $(Ca_{1-x}Y_x)F_{2+x}$ with $x = 0.06$ are presented. A stringent test of the

* To whom correspondence should be addressed.

0022-4596/92 $5.00

Copyright © 1992 by Academic Press, Inc.
All rights of reproduction in any form reserved.

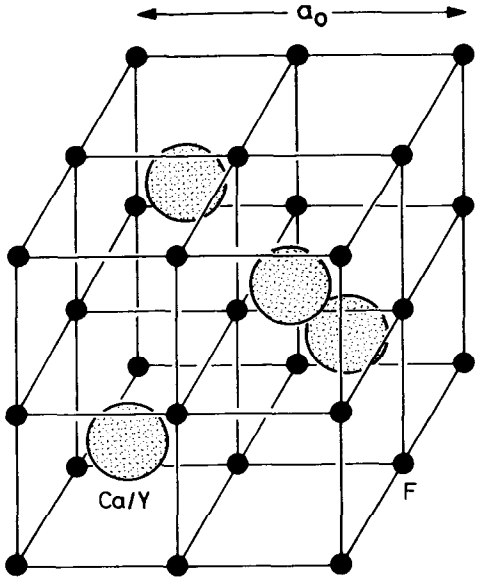

FIG. 1. The fluorite crystal structure.

various defect models proposed in the literature is provided by the combined analysis of both the Bragg scattering, which gives information on the average contents of the unit cell, and the coherent diffuse scattering arising from short-range correlations between disordered ions.

2. Defect Cluster Models

The pioneering neutron diffraction measurements of Cheetham and others (*4–6*) investigated powder and single-crystal samples of $(Ca_{1-x}Y_x)F_{2+x}$, with $0.06 \leq x \leq 0.32$. Analysis of the Bragg intensities indicated that a significant fraction of lattice anion sites are vacant. The displaced and excess anions were found to be distributed in one of two sites, which we denote by F1 and F2. These are situated in Wyckoff sites 48*i* at ($\frac{1}{2}$, *u*, *u*) with $u \approx 0.38$ and 32*f* at (*w*, *w*, *w*) with $w \approx 0.40$, respectively. Subsequent reanalysis of the original published data confirmed the presence of these sites, though with differing site occupancies (*7*). In contrast, a recent study using an $x = 0.10$ sample favors a one-position model containing only F1 sites (*8*). Fourier difference analysis, again using the original diffraction data, provided evidence for a further disordered site, termed F3, in 32*f* at (*v*, *v*, *v*) with $v \approx 0.29$ (*9*, *10*). The proximity of the F3 position to the regular lattice sites at ($\frac{1}{4}$, $\frac{1}{4}$, $\frac{1}{4}$) suggests that these are associated with slight relaxations of surrounding lattice anions toward empty cube centers. The location of the F1 to F3 sites with respect to the regular fluorite lattice is illustrated in Fig. 2, together with the 4*b* sites in empty cube centers at ($\frac{1}{2}$, $\frac{1}{2}$, $\frac{1}{2}$) positions which are termed F4 in this work.

Following the initial identification of the locations of disordered F^- ions on F1 and F2 sites, a series of defect clusters were proposed, comprising F1–F1 interstitial pairs in ⟨110⟩ directions (*4–6*). The simplest of these, which we call Ia, has one F1–F1 pair and is illustrated in Fig. 3a. The presence of F1 anions causes the two nearest neighbor lattice anions to relax in ⟨111⟩ directions into F2 sites, as shown. A series of

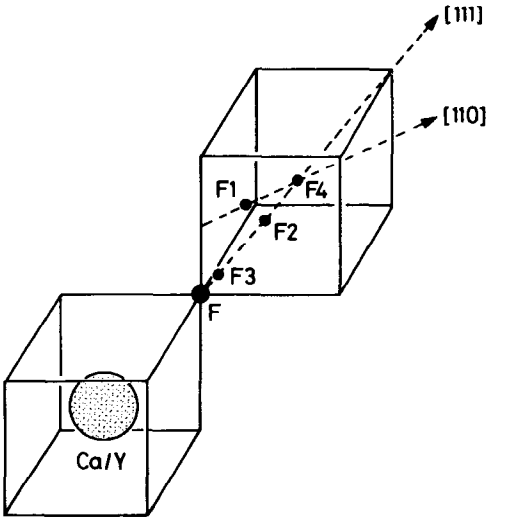

FIG. 2. The location of the disordered anion sites F1 to F4 with respect to the regular fluorite lattice.

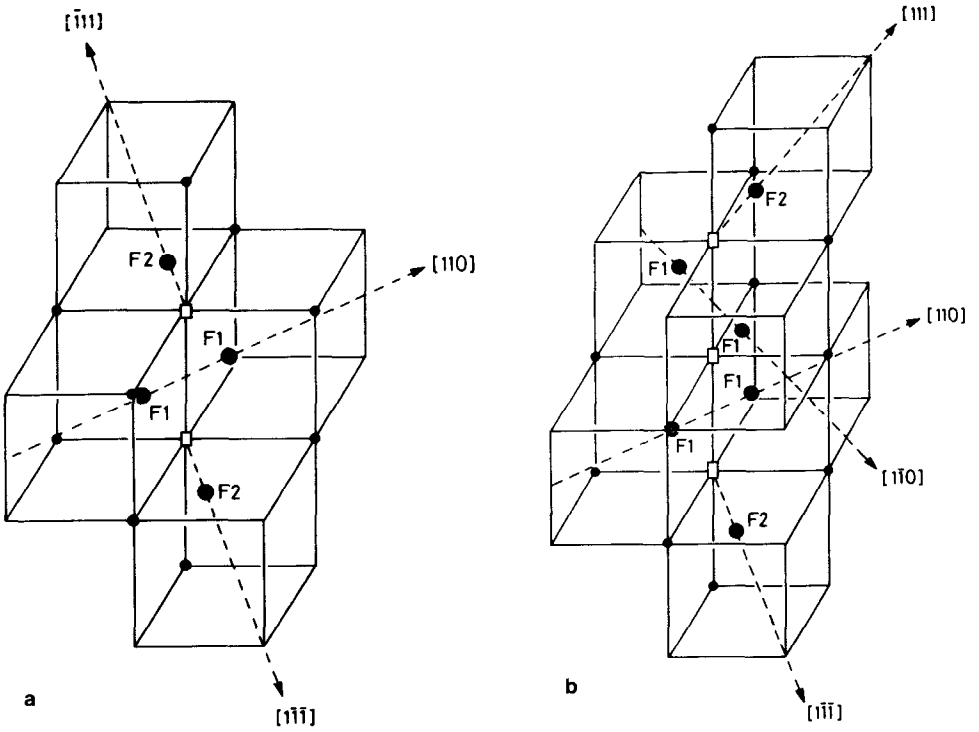

FIG. 3. Schematic diagram of the single (a) and extended (b) ⟨110⟩ pair clusters (*4–6*). These are referred to as model Ia and Ib in the text. The presence of the anions on the F1 sites causes relaxation of the nearest neighbor F2 sites and next nearest neighbor F3 sites away from the defect center in ⟨111⟩ directions toward empty cube centers. For clarity the F3 anions are shown by the symbol ● on the unrelaxed lattice position.

extended clusters containing further F1–F1 pairs were also suggested, which form model Ib, with two alternating F1 pairs (illustrated in Fig. 3b), and model Ic, comprising three F1 pairs. Models Ia and Ib were found to provide the best agreement with the derived occupancies for the F1 and F2 sites at $x = 0.06$–0.10, with the more extended clusters being favored at higher dopant levels (*5, 6*). Probable locations of the next nearest neighbor lattice anions, which are relaxed into F3 sites, are shown in Figs. 3a and 3b. Subsequent neutron scattering investigations of the anion-excess fluorites $(Ca_{1-x}La_x)F_{2+x}$ (*11*), $(Ba_{1-x}La_x)F_{2+x}$ (*12, 13*), and $(Ba_{1-x}U_x)F_{2+2x}$ (*14*) have also been interpreted in terms of defect clusters of type I.

A potential difficulty associated with the type I clusters described above concerns the anomalously short (<2 Å) F1–F1 distances. The apparent absence of very short $F^- - F^-$ distances of this nature in any ordered fluorite compounds led Laval and Frit (*7*) to suggest an alternative series of defect clusters based on the conversion of a single $(Ca,Y)F_8$ fluorite cube into a square antiprism. This produces four anions on F1 sites and four vacancies on regular lattice F sites. Models IIa to IId result from the incorporation of between one and four excess anions along ⟨111⟩ directions into F2 sites, in the enlarged empty cubes adjacent to the transformed face. Model IIa is illustrated in Fig. 4. Surrounding lattice anions are again expected to relax into F3 positions due to the

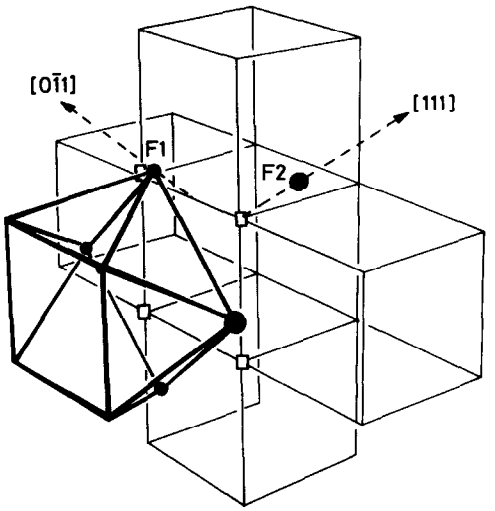

FIG. 4. Schematic diagram of the square antiprism cluster (7) with one additional anion in an F2 site which forms model IIa. Clusters with two, three, and four F2 sites occupied correspond to models IIb, IIc, and IId, respectively. For clarity, the locations of the surrounding lattice anions which relax away from the defect center into F3 sites are not shown.

proximity of an F1 or F2 anion, though for clarity these are not shown in Fig. 4.

It has been suggested (*15*) that the excess anions within dilute $(Ca_{1-x}Y_x)F_{2+x}$ are accommodated in the form of cuboctahedral anion complexes of the type identified in several ordered anion-excess fluorites which are formed at higher dopant levels (*15–19*). This defect is formed by the conversion of six edge-sharing $(M^{2+}, R^{3+})X_8^-$ fluorite cubes into six corner-sharing square antiprisms. This process accommodates four additional X^- anions. The inner faces of these antiprisms form a cuboctahedral polyhedron of 12 X^- anions in F1 sites. Experimental evidence for these clusters has been provided by EXAFS (*20–22*) and powder neutron diffraction (*23, 24*) studies of certain lanthanide-doped CaF_2 systems and single-crystal neutron diffraction studies of $(Sr_{1-x}Pr_x)Cl_{2+x}$ (*9*) and $(Sr_{1-x}Y_x)Cl_{2+x}$ (*25*). Furthermore, computer simulation techniques indicate that cuboctahedral clusters are more stable than type I clusters, particularly for the case of small trivalent cations and if additional anions are located within the central cavity (*26*). The simple cuboctahedral type defect cluster is referred to as model IIIa (Fig. 5). In model IIIb the central cavity is occupied by a fifth additional anion, which is located in an F4 site, and model IIIc contains two extra anions in F2 sities along the ⟨111⟩ direction of the fluorite lattice.

3. Theory

Information concerning the defect structure of disordered compounds is provided by both Bragg diffraction and coherent diffuse scattering measurements. Whilst the former gives information on the positions

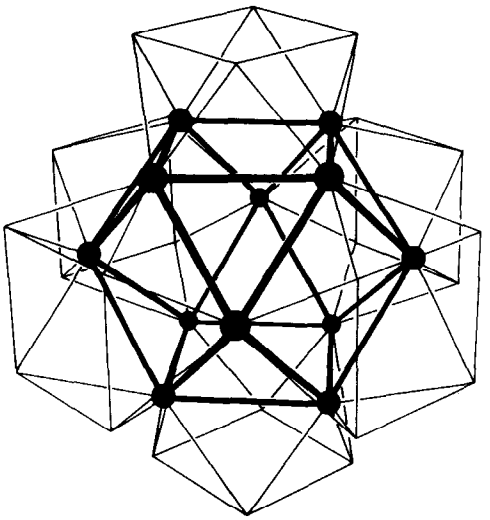

FIG. 5. Schematic diagram of the cuboctahedral defect cluster formed by the conversion of six edge-sharing (Ca, Y)F_8 fluorite cubes into corner sharing square antiprisms. Model IIIa is illustrated; the addition of a single F4 anion in the center and a pair of F2 anions along the ⟨111⟩ direction gives models IIIb and IIIc, respectively. For clarity, the locations of the surrounding lattice anions which relax away from the defect center into F3 sites are not shown.

and mean occupancies of the various crystallographic sites within the unit cell, the latter can provide direct information concerning the local defect configuration.

The coherent elastic neutron scattering from a perfect crystal containing N_a atoms is given by

$$Y(\mathbf{Q}) = \left| \sum_{j=1}^{N_a} b_j \exp(i\mathbf{Q}\cdot\mathbf{R_j}) \exp(-W_j(\mathbf{Q})) \right|^2, \quad (1)$$

where the scattering vector $\mathbf{Q}$ is defined as $\mathbf{Q} = \mathbf{k_i} - \mathbf{k_f}$ and $\mathbf{k_i}$ and $\mathbf{k_f}$ are the wavevectors of the incident and scattered beams, respectively. $\mathbf{R_j}$ is the position vector of the jth atom, which has a coherent neutron scattering length b_j, and the term $\exp(-W_j(\mathbf{Q}))$ is the usual Debye–Waller temperature factor for atom j.

For a perfect crystal containing a small number, N_d, of identical defect clusters we rewrite Eq. (1) as

$$Y(\mathbf{Q}) = \left| \sum_{j=1}^{N_a} b_j \exp(i\mathbf{Q}\cdot\mathbf{R_j}) \exp(-W_j(\mathbf{Q})) + \sum_{k=1}^{N_c} P_k b_k \exp(i\mathbf{Q}\cdot\mathbf{R_k}) \exp(-W_k(\mathbf{Q})) \right|^2. \quad (2)$$

The first term in Eq. (2) is a summation over the undistorted sites in the crystal and the second term contains all the N_c disordered sites, with $P_k = -1$ for a lattice site vacancy and $P_k = 1$ for an interstitial atom. An atom relaxed from its regular lattice site is formally equivalent to a vacancy at $\mathbf{R_k} = \mathbf{R_j}$ plus an interstitial at $\mathbf{R_k}$. Similarly, a substitutional impurity is treated as a vacancy and interstitial on identical sites, though with differing values of b_k and, possibly, $W_k(\mathbf{Q})$. Expansion of Eq. (2) gives four terms, the first of which corresponds to Bragg scattering from a perfect crystal and is zero except at the reciprocal lattice points $\mathbf{Q} = \tau$. This term may be written as

$$Y_B(\mathbf{Q}) = N_u(2\pi)^3/V_u \, |F_B(\mathbf{Q})|^2 \delta(\mathbf{Q} - \tau), \quad (3)$$

where the subscript B denotes Bragg scattering. The structure factor $F_B(\mathbf{Q})$ now contains the summation over the n_u atoms in one of the (identical) N_u unit cells, which each have volume V_u.

$$F_B(\mathbf{Q}) = \sum_{j=1}^{n_u} b_j \exp(i\mathbf{Q}\cdot\mathbf{r_j}) \exp(-W_j(\mathbf{Q})), \quad (4)$$

where $\mathbf{r_j}$ is now the position vector of the jth atom inside the unit cell. The two cross terms in the expansion of Eq. (2) describe the effect of disorder on the Bragg intensity $Y_B(\mathbf{Q})$. This modifies the structure factor to represent the mean contents of the unit cell, averaged over the whole crystal, so that

$$F_B(\mathbf{Q}) = \sum_{j=1}^{n_u} m_j b_j \exp(i\mathbf{Q}\cdot\mathbf{r_j}) \exp(-W_j(\mathbf{Q})), \quad (5)$$

where the summation over n_u now includes all the occupied sites, which have an average occupancy m_j. The final term in the expansion describes the distribution of coherent diffuse scattering over reciprocal space $\mathbf{Q}$ caused by the presence of defect clusters within the crystal. For a dilute concentration of clusters the scattering from each of the N_d defects is summed incoherently and

$$Y_D(\mathbf{Q}) = N_d |F_D(\mathbf{Q})|^2 \quad (6)$$

The structure factor for the defect cluster is given by

$$F_D(\mathbf{Q}) = \sum_{k=1}^{n_c} P_k b_k \exp(i\mathbf{Q}\cdot\mathbf{R_k}) \exp(-W_k(\mathbf{Q})), \quad (7)$$

where n_c is the number of defective ions (including vacancies) in a single defect clus-

ter. Equations (3) and (6) describe the scattered intensity due to Bragg scattering at $\mathbf{Q} = \tau$ and diffuse scattering at all $\mathbf{Q}$, respectively.

4. Experimental

The neutron scattering measurements were performed on two fragments of a single-crystal boule of $(Ca_{1-x}Y_x)F_{2+x}$ with $x = 0.06$ grown from the melt by Dr. R. C. C. Ward of the Clarendon Laboratory Crystal Growth Group, University of Oxford. The boule was slowly cooled to ambient temperature. For these systems, the thermal history of the sample is relatively unimportant (*6*) and no subsequent annealing of the sample was performed. A dopant concentration of $x = 0.06$ was chosen to allow direct comparisons with the earlier work on the $(Ca_{1-x}Y_x)F_{2+x}$ system (*4–6*) and to conform to the requirement of isolated defects imposed by Eq. (6). For measurement of the Bragg intensities a small cylindrical crystal of approximately 3 mm diameter and 9 mm length was used, to avoid excessive extinction of the diffracted beam. The distribution of the relatively weak coherent diffuse scattering features observed elsewhere in reciprocal space was measured using a larger crystal of approximately 12 mm diameter and 25 mm length. Both crystals had the $[1\bar{1}0]$ axis along the length of the cylinder and were mounted on the diffractometer with this crystallographic direction vertical.

Data were collected on the single crystal diffractometer (SXD) at the ISIS Spallation Neutron Source (*27*). This instrument is a time-of-flight Laue diffractometer which exploits the pulsed nature of the incident flux and uses a large area position-sensitive detector (PSD) to measure large volumes of reciprocal space at each crystal setting. The Bragg diffraction and diffuse scattering measurements were performed with the same experimental configuration. The PSD used has an active area of 80 mm × 80 mm with each pixel having 5 mm × 5 mm spatial resolution. At its distance of 0.25 m the detector subtends an angular range of some 20° × 20° at the sample. All measurements were performed with the central pixel at $2\theta = 90°$ and in the horizontal scattering plane. The crystals were rotated in steps of $\omega = 8°$ using neutrons in the wavelength range $0.48 > \lambda > 8.63$ Å, recorded using the time-of-flight technique. Adequate counting statistics for the Bragg diffraction and diffuse scattering measurements were collected after approximately 2 and 3 hr counting times, respectively.

A total of 124 Bragg reflections were measured, out to a maximum of $\sin\theta/\lambda = 1.47$ Å^{-1}. Intensities were extracted using standard procedures and normalized to remove the wavelength dependence of the incident neutron flux. This process uses the intensity measured from a polycrystalline vanadium sample (which scatters neutrons incoherently) measured with the same experimental configuration. Following the application of wavelength-dependent extinction and reflectivity corrections, a total of 75 independent Bragg intensities $I_B(hkl)$ were obtained by averaging over equivalent reflections. No corrections for thermal diffuse scattering (T.D.S.) were applied to the $I_B(hkl)$ data.

Preliminary investigations of the distribution of coherent elastic diffuse scattering indicated that the intensity lies predominantly in the $(1\bar{1}0)$ plane of reciprocal space, corresponding to scattering approximately in the horizontal plane of the detector. The time-of-flight spectra for the horizontal pixels were normalized using the same vanadium sample procedure discussed above. The normalized diffuse intensity, $I_D(\mathbf{Q})$ was mapped onto the $(1\bar{1}0)$ plane of reciprocal space and stored as a two-dimensional array with the x and y axes corresponding to the $[hh0]$ and $[00l]$ reciprocal space directions, respectively. h and l cover the ranges from 0.0 to 4.0 and from 0.0 to 6.0, respectively, both in steps of 0.1 reciprocal lattice units.

Close to the reciprocal lattice points $\mathbf{Q} = \tau$ the intensity is obscured by Bragg scattering and these points were excluded from the diffuse scattering analysis, leaving a total of 2431 individual data points.

Full matrix least-squares refinement of the intensity data for both $I_B(hkl)$ and $I_D(\mathbf{Q})$ were performed, where the χ^2 function minimized is defined by

$$\chi^2 = R_w^2/R_{exp}^2 \tag{8}$$

and the weighted R-factor is given by

$$R_w^2 = \sum_{i=1}^{N_d} (w_i(I_{obs,i} - I_{calc,i}))^2 \Big/ \sum_{i=1}^{N_d} (w_i I_{obs,i})^2, \tag{9}$$

where the weights w_i are taken to be the reciprocal of the square of the standard deviation ($w_i = 1/\sigma I_{obs,i}$) of each of the N_d observations. The expected R-factor is given by

$$R_{exp}^2 = (N_d - N_p)^2 \Big/ \sum_{i=1}^{N_d} (w_i I_{obs,i})^2, \tag{10}$$

where N_p is the number of fitted parameters. Estimated errors on the fitted parameters are obtained from the covariance matrix in the standard manner(*28*).

Following the expressions derived in Section 3, the calculated Bragg intensity is given by

$$I_{B,calc}(hkl) = S_B|F_B(\mathbf{Q})|^2, \tag{11}$$

where S_B is the fitted scale parameter and the Bragg structure factor $F_B(\mathbf{Q})$ is given by Eq. (5). The corresponding expression for the diffuse scattering intensity is

$$I_{D,calc}(\mathbf{Q}) = C + (S_D/N_o) \sum_{i=1}^{N_o} |F_D(\mathbf{Q})|^2, \tag{12}$$

where the $F_D(\mathbf{Q})$ is given by Eq. (7). Since the defect clusters often possess lower symmetry than the host fluorite lattice the structure factor for the clusters must be averaged over the N_o possible reorientations of the defect. The fitted constant C is included to account for the measured scattering due to instrumental background, multiple scattering and incoherent scattering, and is assumed to be independent of $\mathbf{Q}$.

5. Results

Examination of the observed Bragg intensities confirmed that the systematic absences were consistent with $Fm\bar{3}m$ space group symmetry. Least-squares refinements of the Bragg intensity data for $I_B(hkl)$ were undertaken using coherent scattering lengths of $b(Ca) = 0.490 \times 10^{-12}$ cm, $b(Y) = 0.775 \times 10^{-12}$ cm, and $b(F) = 0.565 \times 10^{-12}$ cm (*29*). The 4*a* cation sites were assumed to be randomly occupied by Ca and Y in the ratio 0.94 : 0.06 given by the chemical composition.

Initial refinement using a physically unrealistic model with full occupancy of the fluorine sublattice and no excess anions sites produced a value $\chi^2 = 5.03$. Subsequent analysis allowed F^- anions to occupy the four disordered sites F1 to F4 which were discussed in Section 2 and illustrated in Fig. 2. Refinements were undertaken varying each site in turn, with overall charge neutrality imposed by constraint of the total fluorine occupancy to $m = 2.06$. The thermal vibrations of the lattice fluorine anions were assumed to be anisotropic, though the disordered anions were constrained to vibrate isotropically. Significant reductions in χ^2 were only provided by introduction of the F1 and F3 sites, to values of 3.40 and 3.94, respectively. Although some correlations were present between the thermal vibration parameters and site occupancies of the disordered anion sites it proved possible to obtain a stable minimization with $\chi^2 = 2.79$ ($R_w = 5.54\%$) with all the F1 to F4 site occupancies refined simultaneously. The final values of the fitted structural and thermal parameters are given in Table I.

It is informative at this stage to compare

TABLE I

THE STRUCTURAL AND THERMAL VIBRATION PARAMETERS OF $(Ca_{1-x}Y_x)F_{2+x}$ WITH $x = 0.06$ DETERMINED BY LEAST-SQUARES REFINEMENT OF THE BRAGG INTENSITIES

Atom	Site	Position	Parameter
$Ca_{0.94}Y_{0.06}$	4*a*	(0, 0, 0)	$B_{iso} = 0.64(1)$ Å^2
F	8*c*	$(\frac{1}{4}, \frac{1}{4}, \frac{1}{4})$	$m = 1.59(9)$
			$B_{11} = 0.60(7)$ Å^2
			$B_{33} = 0.81(9)$ Å^2
F1	48*i*	$(\frac{1}{2}, u, u)$	$u = 0.390(5)$
			$m = 0.16(2)$
			$B_{iso} = 1.4(4)$ Å^2
F2	32*f*	(w, w, w)	$w = 0.38(3)$
			$m = 0.01(2)$
			$B_{iso} = 2.2(43)$ Å^2
F3	32*f*	(v, v, v)	$v = 0.270(8)$
			$m = 0.31(5)$
			$B_{iso} = 1.1(2)$ Å^2
F4	4*b*	$(\frac{1}{2}, \frac{1}{2}, \frac{1}{2})$	$m = 0.01(3)$
			$B_{iso} = 3.2(55)$ Å^2

Note. The occupancies, *m*, are given as the contribution to the overall fluorine content, 2.06.

the results obtained in this work with those reported previously. For the $x = 0.06$ case, a striking discrepancy concerns the F2 site, which was found to have a significant occupancy in the original study (*4–6*) and the subsequent reanalyses of the original data (*7, 9, 10*). The apparent absence of anions on the F2 sites is, however, supported by the most recent work using a dopant concentration of $x = 0.10$ (*8*). The uncertainties regarding the occupancies of disordered sites within anion-excess fluorites have important consequences for their subsequent interpretation in terms of different defect models and have been addressed in detail elsewhere (*10, 30*). It has been suggested that, under certain circumstances, the observation of F2 type sites within anion-excess fluorites can be an artefact of the data analysis procedure (*30*). It is argued that the presence of scattering intensity associated with the F2 site at ~(0.42, 0.42, 0.42) can result from the overlap of the three F1 peaks at $(\frac{1}{2}, 0.38, 0.38)$, $(0.38, \frac{1}{2}, 0.38)$, and $(0.38, 0.38, \frac{1}{2})$ distributed around the threefold axis. Furthermore, ambiguities in the derived occupancies can be induced by constraint of the thermal parameters of the disordered sites (*10*), underlining the importance of high-**Q** diffraction data in minimizing the correlations between the occupancies of disordered sites and their thermal vibration parameters.

The potential difficulties outlined in the previous paragraph demonstrate the importance of single-crystal measurements for these studies and, in particular, the use of coherent diffuse scattering to investigate directly the short-range correlations between disordered sites. With the more limited datasets available using powder diffraction (*23, 24*) the problems are compounded by the loss of information due to overlap of the $h + k + l = 4n \pm 1$ reflections which, if distinguished, permit decorrelation of anharmonic thermal vibrations and static disorder due to relaxed lattice anions.

Figure 6 illustrates the distribution of the coherent diffuse intensity $I_D(\mathbf{Q})$ observed in the $(1\bar{1}0)$ plane of reciprocal space. Preliminary calculations of the diffuse scattering within $(Ca_{1-x}Y_x)F_{2+x}$ produced by the various models indicated that the intensity distribution is predominantly determined by the disordered anions. Consequently, the locations of the substitutional yttrium dopant cations within the defect clusters are not considered in this work. Least-squares minimization of the diffuse scattering data $I_D(\mathbf{Q})$ based on each model was initially undertaken with the positional and thermal vibration parameters fixed at the values given by the Bragg scattering analysis (Table I). Subsequent refinements allowed these parameters to vary from these starting values. The final value of χ^2 for each model is listed in Table II, together with the significant changes in parameter values observed. The relatively high χ^2 results from the poor fit in the vicinity of reciprocal lattice points. This

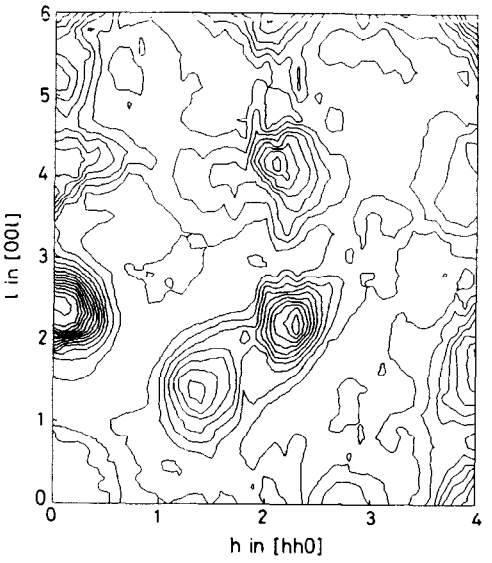

FIG. 6. The measured coherent diffuse scattering in the (1$\bar{1}$0) plane of reciprocal space caused by the presence of defect clusters within the $(Ca_{1-x}Y_x)F_{2+x}$ single-crystal sample.

is due to inelastic scattering from low energy acoustic phonon modes and, to a lesser extent, from neglect of the disorder on the cation sites due to the Y^{3+} doping. The best overall fit to the diffuse scattering data is obtained using model III. The final fitted pattern obtained from model IIIb is shown in Fig. 7 and may be compared with the measured pattern in Fig. 6.

6. Discussion

The low occupancy of the disordered F2 site determined from the analysis of the Bragg scattering data cannot easily be reconciled with the presence of defect clusters of type I and II within anion-excess $(Ca_{1-x}Y_x)F_{2+x}$. Table III provides a direct comparison between the experimental site occupancies and those calculated for each defect cluster model. The calculated values underlined in Table III are those which lie within the estimated errors on the experimental values. It is clear that only models IIIa and IIIb successfully account for all the observed occupancies. However, in view of the uncertainty concerning the presence of disordered anions on the F2 sites discussed in the previous section, the site occupancies alone cannot be taken as conclusive evidence that only clusters of these types are present within the solid solution.

TABLE II

VALUES OF THE GOODNESS-OF-FIT PARAMETER χ^2, DEFINED IN EQ. (8), OBTAINED BY LEAST-SQUARES FITTING OF THE COHERENT DIFFUSE SCATTERING DATA

Model	Description	χ^2 (a)	χ^2 (b)	Remarks
Ia	1 ⟨110⟩ F1 pair	43.7	34.1	$u \rightarrow -0.45$, $B_{iso}(F2) \rightarrow -10$ Å^2
Ib	2 ⟨110⟩ F1 pairs	47.3	31.0	"
Ic	3 ⟨110⟩ F1 pairs	57.1	42.6	"
IIa	Antiprism + 1 F2	29.7	25.6	$w \rightarrow -0.30$
IIb	Antiprism + 2 F3	31.6	24.6	"
IIc	Antiprism + 3 F2	35.1	29.2	$w \rightarrow -0.45$
IId	Antiprism + 4 F2	38.4	30.9	$w \rightarrow -0.47$, $B_{iso}(F1) \rightarrow -9$ Å^2
IIIa	Cuboctahedron	20.3	17.6	$v \rightarrow -0.265$, $B_{iso}(F1) \rightarrow -1.9$ Å^2
IIIb	Cuboct. + central F4	19.6	16.8	"
IIIc	Cuboct. + ⟨111⟩ F2 pair	20.6	17.9	"

Note. Column (a) gives the χ^2 obtained for each model with the positional and thermal vibration parameters fixed at the values given by the analysis of the Bragg scattering data (Table I). Column (b) gives the χ^2 obtained when these are allowed to vary, followed by brief details of the significant parameter changes observed.

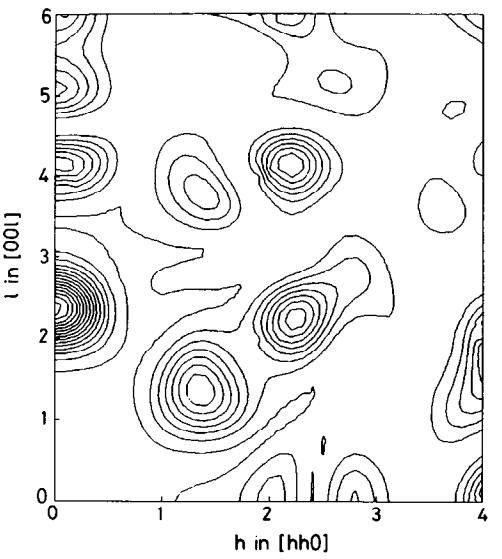

FIG. 7. The calculated coherent diffuse scattering in the (1$\bar{1}$0) plane of reciprocal space assuming a random distribution of cuboctahedral defect clusters of type IIIb. The values of the positional and thermal vibration parameters are obtained by least-squares refinement of the experimental data shown in Fig. 6.

An additional requirement placed on the proposed models concerns the interionic distances between the various anions. For each defect cluster these have been calculated using the refined positional parameters and are listed in Table IV. For comparison, the F^-–F^- distance based on the ionic radius is 2.62 Å (*31*) whilst in pure CaF_2 it is 2.73 Å. As noted previously (*7*), defect clusters of type I include very short distances between the F1 anions and the relaxed nearest neighbor anions in F2 sites and between the two F1 anions. Although the former distance is subject to some experimental uncertainty, owing to the minimal occupancy of the F2 sites, the F1–F1 distance in ⟨110⟩ directions requires explanation. Computer simulation techniques (*32*) have suggested that shorter F^-–F^- distances can occur if an additional covalent attraction produces an F_2^{2-} complex. However, anomalously short anion–anion distances are not observed in ordered fluorite compounds and defect models which include F^-–F^- distances significantly shorter than ~2.3 Å must be treated with some reservation. Model II does not contain any anomalously short F^-–F^- distances and model IIIa has no distances shorter than 2.63 Å. The values for model IIIb in Table IV indicate that there is sufficient space inside the central cuboctahedral cavity to ac-

TABLE III

COMPARISON OF THE CALCULATED VALUES OF THE ANION SITE OCCUPANCIES, BASED ON THE VARIOUS DEFECT MODELS DESCRIBED IN THE TEXT, AND THE RESULTS OBTAINED FROM LEAST-SQUARES ANALYSIS OF THE BRAGG SCATTERING DATA

Model	Description	F ($\frac{1}{4}$, $\frac{1}{4}$, $\frac{1}{4}$)	F1 ($\frac{1}{2}$, u, u)	F2 (w, w, w)	F3 (v, v, v)	F4 ($\frac{1}{2}$, $\frac{1}{2}$, $\frac{1}{2}$)
Ia	1 ⟨110⟩ F1 pair	1.640	0.060	0.060	0.300	0.000
Ib	2 ⟨110⟩ F1 pairs	1.760	0.060	0.030	0.210	0.000
Ic	3 ⟨110⟩ F1 pairs	1.780	0.060	0.020	0.200	0.000
IIa	Antiprism + 1 F2	1.340	0.240	0.060	0.420	0.000
IIb	Antiprism + 2 F2	1.580	0.120	0.060	0.300	0.000
IIc	Antiprism + 3 F2	1.660	0.080	0.060	0.260	0.000
IId	Antiprism + 4 F2	1.700	0.060	0.060	0.240	0.000
IIIa	Cuboctahedron	1.520	0.180	0.000	0.360	0.000
IIIb	Cuboct. + central F4	1.616	0.144	0.000	0.288	0.012
IIIc	Cuboct. + ⟨111⟩ F2 pair	1.680	0.120	0.020	0.240	0.000
Bragg diffraction analysis		1.59(9)	0.16(2)	0.01(2)	0.31(5)	−0.01(3)

Note. The calculated occupancies which lie within the errors on the experimental values are underlined.

TABLE IV

VALUES OF THE F^-–F^- INTERIONIC DISTANCES (IN Å) FOR THE VARIOUS DEFECT MODELS DESCRIBED IN THE TEXT

Model	F–F	F1–F1	F2–F2	F2–F1	F2–F	F3–F3	F3–F2	F3–F1	F3–F	F4–F1
Ia → c	2.74	2.17	—	1.62	2.95	2.96	3.70	2.64	2.63	—
IIa → d	2.74	3.02	—	2.55	2.95	2.96	2.37	2.64	2.63	—
IIIa	2.74	3.02	—	—	—	2.96	—	2.64	2.63	—
IIIb	2.74	3.02	—	—	—	2.96	—	2.64	2.63	3.02
IIIc	2.74	3.02	2.28	1.62	—	2.96	—	2.64	2.63	—

Note. Distances which are significantly shorter than those observed in ordered anion-excess fluorites are underlined. The estimated error on the distances is ±0.04 Å except in the case of distances involving the rather poorly determined F2 sites where the error is ~ ±0.15 Å.

commodate a central F4 anion. However, this is not the case for a ⟨111⟩ pair of F2 anions as required in model IIc and this model must therefore be rejected.

Least-squares refinements of the diffuse scattering data, summarized in Table II, clearly favor the presence of cuboctahedral clusters of type III. For models I and II a significant improvement in the quality of the fit is obtained by allowing the positional and thermal vibration parameters to vary away from those obtained from the Bragg intensity analysis. In all cases, however, the fitted parameters adopt physically unrealistic values which result in excessively short F^-–F^- distances and in some cases anomalously large thermal vibration parameters. The full refinements of the type III defects produce a slight improvement in χ^2, with the lowest value obtained using model IIIb. A comparison of the results obtained from the Bragg and diffuse scattering analysis using model IIIb is given in Table V. The excellent agreement between the two independent analyses strongly supports our conclusion that the disordered structure of the $(Ca_{1-x}Y_x)F_{2+x}$ solid solution comprises predominantly cuboctahedral-type defect clusters. The absence of broad diffuse scattering intensity in other regions of reciprocal space provides no evidence for the presence of additional smaller defect clusters, such as fragments of cuboctahedral units.

The relatively large experimental uncertainty concerning the F4 site occupancy derived from the Bragg analysis (Table I) does not provide any conclusive information concerning the presence of an additional central anion inside the cuboctahedral cavity. Likewise, there is only a slight improvement in the quality of fit to the diffuse scattering data using model IIIb rather than IIIa. Simple geometric considerations show that the conversion of a fluorite cube to a square antiprism gives a positional parameter $u = \frac{1}{4}\sqrt{2} = 0.354$ for the F1 site (*33*). The somewhat higher value observed, $u = 0.390(5)$, may provide indirect evidence of a central anion since Coulombic repulsion might be expected to enlarge the cuboctahedral cavity. The increased value of u also explains the presence of relaxed nearest neighbor anions in F3 sites, which helps to avoid unacceptably short F^-–F^- distances.

There has recently been considerable interest in the structural properties of the ordered anion-excess compounds, with increased evidence that cuboctahedral anion complexes are a fundamental structural unit in these fluorite superlattices (*33–35*). The conversion of six edge-sharing fluorite cubes into six corner-sharing square antiprisms replaces a $(M^{2+}, R^{3+})_6X_{32}^-$ fluorite fragment by $(M^{2+}, R^{3+})_6X_{36}^-$, or $(M^{2+}, R^{3+})_6X_{37}^-$ if the central cuboctahedral cavity is occupied by a further anion. The latter process accommo-

TABLE V

COMPARISON BETWEEN THE VALUES OF POSITIONAL AND THERMAL VIBRATION PARAMETERS OBTAINED FROM THE LEAST-SQUARES ANALYSIS OF THE BRAGG AND DIFFUSE SCATTERING DATA

Atom	Position	Bragg	Diffuse
F1	$(\frac{1}{2}, u, u)$	$u = 0.390(5)$	$u = 0.384(3)$
		$B_{iso} = 1.4(4)$ Å^2	$B_{iso} = 1.86(8)$ Å^2
F3	(v, v, v)	$v = 0.270(8)$	$v = 0.265(5)$
		$B_{iso} = 1.1(2)$ Å^2	$B_{iso} = 1.21(5)$ Å^2
F4	$(\frac{1}{2}, \frac{1}{2}, \frac{1}{2})$	$B_{iso} = 3.2(55)$ Å^2	$B_{iso} = 4.6(33)$ Å^2

Note. The latter are those obtained using model IIIb.

dates five additional anions into the structure and different packings of these polyhedra then lead to a homologous series of ordered compounds, $M^{2+}_{m-5}R^{3+}_5X^-_{2m+5}$. In the CaF_2–YF_3 system full structural determination has only been reported for the $m = 19$ member (*15*), which has been identified as the naturally occurring mineral tveitite, of approximate composition $Ca_{14}Y_5F_{43}$. In this structure the (Ca, Y)$_6F_{37}$ units are distributed along the threefold axis, leading to $R\bar{3}$ symmetry, and are separated by fragments of relatively undistorted fluorite lattice. Further evidence for such structural units is provided by their identification in Ca_2YbF_7 (*16–18*) and Ca_2LuF_7 (*22*), which appear to be isostructural with the $m = 15$ member Ca_2YF_7, and in $Na_7Zr_6F_{31}$, which has been suggested as isostructural with the $m = 13$ member $Ca_8Y_5F_{31}$ (*36*).

Our results, therefore, indicate that the solid solution phase of $(Ca_{1-x}Y_x)F_{2+x}$ contains randomly distributed defect clusters, predominantly of the cuboctahedral type. These become ordered over three dimensions as the concentration of trivalent cations increases and induces the formation of the various fluorite superlattice phases. This is consistent with the observation that the mineral tveitite often exists as an intergrowth of the ordered phase and the fluorite solid solution (*15*). Finally, it is interesting to note that this behavior mirrors that observed in the anion-deficient fluorite compounds where, for example, clusters of vacancy pairs found in the $(Zr_{1-x}Y_x)O_{2-x/2}$ disordered solid solution (*37–39*) can be considered as fragments of the ordered structure of the compound $Zr_3Y_4O_{12}$ (*40*).

7. Conclusions

In summary, measurements of the Bragg and coherent diffuse neutron scattering from single-crystal $(Ca_{1-x}Y_x)F_{2+x}$ with $x = 0.06$ indicate that the predominant defect species present in the disordered fluorite lattice comprises cuboctahedral anion clusters, formed by the combined conversion of six edge-sharing (Ca, Y)F_8 fluorite cubes into six corner-sharing square antiprisms. This model provides the best overall agreement with the observed occupancies of the disordered anion sites at $(\frac{1}{2}, u, u)$ with $u = 0.390(5)$ and (v, v, v) with $v = 0.270(8)$. This cuboctahedral defect does not include any anomalously short $F^- - F^-$ contacts of the type obtained if other defect cluster models are adopted. Least-squares refinement of the distribution of coherent diffuse intensity over reciprocal space supports the presence of cuboctahedral clusters and gives refined positional and thermal vibration parameters in excellent agreement with those obtained from the analysis of the Bragg scattering data. These clusters are distributed randomly within the fluorite

solid solution and possess a structure which is strongly related to the polyhedral complexes which form the basis of many ordered anion-excess fluorites.

Acknowledgments

We are grateful to R. C. C. Ward of the Clarendon Laboratory Crystal Growth Group, University of Oxford, for supplying the single-crystal specimens used in this work. We are also indebted to Z. A. Bowden for her assistance with the collection of the experimental data, to D. A. Keen for suggestions regarding the data reduction procedures, and to J. P. Goff for advice concerning the diffuse scattering calculations.

References

1. C. R. A. Catlow, J. D. Comins, F. A. Germano, R. T. Harley, W. Hayes, and I. B. Owen, *J. Phys. C* **14,** 329 (1981).
2. C. G. Andeen, J. J. Fontanella, M. C. Wintersgill, P. J. Welcher, R. J. Kimble, and G. E. Matthews, *J. Phys. C* **14,** 3557 (1981).
3. U. Ranon and A. Yaniv, *Phys. Rev. Lett.* **9,** 17 (1964).
4. A. K. Cheetham, B. E. F. Fender, D. Steele, R. I. Taylor, and B. T. M. Willis, *Solid State Commun.* **8,** 171 (1970).
5. A. K. Cheetham, B. E. F. Fender, and M. J. Cooper, *J. Phys. C* **4,** 3107 (1971).
6. D. Steele, P. E. Childs and B. E. F. Fender, *J. Phys. C* **5,** 2677 (1972).
7. J. P. Laval and B. Frit, *J. Solid State Chem.* **49,** 237 (1983).
8. L. P. Otroshchenko, V. B. Aleksandrov, N. N. Bydanov, V. I. Simonov, and B. P. Sobolev, *Sov. Phys. Crystallogr.* **33,** 449 (1988).
9. P. J. Bendall, C. R. A. Catlow, and B. E. F. Fender, *J. Phys. C* **17,** 797 (1984).
10. P. J. Bendall, D. Phil. thesis, Oxford (1980).
11. C. R. A. Catlow, A. V. Chadwick, and J. Corish. *J. Solid State Chem.* **48,** 65 (1983).
12. J. K. Kjems, N. H. Andersen, J. Schoonman, and K. Clausen, *Physica* **120B,** 357 (1983).
13. N. H. Andersen, K. N. Clausen, J. K. Kjems, and J. Schoonman, *J. Phys. C* **19,** 2377 (1986).
14. N. H. Andersen, K. Clausen, and J. K. Kjems, *Solid State Ionics,* **9&10,** 543 (1983).
15. D. J. M. Bevan, J. Strähle, and O. Greis, *J. Solid State Chem.* **44,** 75 (1982).
16. S. E. Ness, D. J. M. Bevan, and H. J. Rossell, *Eur. J. Solid State Inorg. Chem.* **25,** 509 (1988).
17. D. J. M. Bevan, M. J. McCall, S. E. Ness, and M. R. Taylor, *Eur. J. Solid State Inorg. Chem.* **25,** 517 (1988).
18. D. J. M. Bevan, S. E. Ness, and M. R. Taylor, *Eur. J. Solid State Inorg. Chem.* **25,** 527 (1988).
19. W. Gettmann and O. Greis, *J. Solid State Chem.* **26,** 255 (1978).
20. C. R. A. Catlow, A. V. Chadwick, G. N. Greaves, and L. M. Moroney, *Nature* **312,** 601 (1984).
21. C. R. A. Catlow, A. V. Chadwick, J. Corish, L. M. Moroney, and A. N. O'Reilly, *Phys. Rev. B* **39,** 1897 (1989).
22. J. P. Laval, A. Mikou, and B. Frit, *J. Solid State Chem.* **85,** 133 (1990).
23. J. P. Laval, A. Mikou, and B. Frit, *Solid State Ionics* **28–30,** 1300 (1988).
24. J. P. Laval, A. Abaouz, and B. Frit, *J. Solid State Chem.* **81,** 271 (1989).
25. J. P. Goff, M. T. Hutchings, S. Hull, B. Fåk, and W. Hayes, *J. Phys.: Condensed Matter* **4,** 1433 (1992).
26. P. J. Bendall, C. R. A. Catlow, J. Corish, and P. W. M. Jacobs, *J. Solid State Chem.* **51,** 159 (1984).
27. C. C. Wilson and D. A. Keen, *in* "ICANS-XI International Collaboration on Advanced Neutron Sources" (N. Watanabe, Ed.), p. 849 KEK Report 90-25, Japan (1991).
28. G. H. Stout and L. H. Jensen, "X-ray Structure Determination. A Practical Guide," Ch. 17, Wiley, New York (1989).
29. L. Koestler and W. B. Yelon, "Summary of Low Energy Neutron Scattering Lengths and Cross Sections," Netherlands Research Foundation, Dept. of Physics, Petten, The Netherlands (1982).
30. L. A. Muradyan, B. A. Maksimov, V. B. Aleksandrov, L. P. Otroshchenko, N. N. Bydanov, M. I. Sirota, and V. I. Simonov, *Sov. Phys. Crystallogr.* **31,** 390 (1986).
31. R. D. Shannon and C. T. Prewitt, *Acta Crystallogr. Sect. B* **25,** 925 (1969).
32. C. R. A. Catlow, *J. Phys. C* **6,** 464 (1973).
33. D. J. M. Bevan and S. E. Lawton, *Acta Crystallogr. Sect. B* **42,** 55 (1986).
34. D. J. M. Bevan, O. Greis, and J. Strähle, *Acta Crystallogr. Sect. A* **36,** 889 (1980).
35. A. M. Golubev and V. I. Simonov, *Sov. Phys. Crystallogr.* **31,** 281 (1986).
36. J. H. Burns, R. D. Ellison, and H. A. Levy, *Acta Crystallogr. Sect. B* **24,** 230 (1968).

37. R. OSBORN, N. H. ANDERSEN, K. CLAUSEN, M. A. HACKETT, W. HAYES, M. T. HUTCHINGS, AND J. E. MACDONALD, *Mater. Sci. Forum* **7,** 55 (1986).
38. N. H. ANDERSEN, K. CLAUSEN, M. A. HACKETT, W. HAYES, M. T. HUTCHINGS, J. E. MACDONALD, AND R. OSBORN, *Physica* **136,** 315 (1986).
39. S. HULL, T. W. D. FARLEY, M. A. HACKETT, W. HAYES, R. OSBORN, N. H. ANDERSEN, K. CLAUSEN, M. T. HUTCHINGS, AND W. G. STIRLING, *Solid State Ionics* **28–30,** 488 (1988).
40. H. G. SCOTT, *Acta Crystallogr. Sect. B* **33,** 281 (1977).